Modeling postshock evolution of large electropores

John C. Neu[1,2] and Wanda Krassowska[2,*]
[1]*Department of Mathematics, University of California at Berkeley, Berkeley, California 94720*
[2]*Department of Biomedical Engineering, Duke University, Durham, North Carolina 27708*
(Received 6 June 2001; revised manuscript received 16 December 2002; published 27 February 2003)

The Smoluchowski equation (SE), which describes the evolution of pores created by electric shocks, cannot be applied to modeling large and long-lived pores for two reasons: (1) it does not predict pores of radius above 20 nm without also predicting membrane rupture; (2) it does not predict postshock growth of pores. This study proposes a model in which pores are coupled by membrane tension, resulting in a nonlinear generalization of SE. The predictions of the model are explored using examples of homogeneous (all pore radii r are equal) and heterogeneous ($0 \leqslant r \leqslant r_{max}$) distributions of pores. Pores in a homogeneous population either shrink to zero or assume a stable radius corresponding to the minimum of the bilayer energy. For a heterogeneous population, such a stable radius does not exist. All pores, except r_{max}, shrink to zero and r_{max} grows to infinity. However, the unbounded growth of r_{max} is not physical because the number of pores per cell decreases in time and the continuum model loses validity. When the continuum formulation is replaced by the discrete one, the model predicts the coarsening process: all pores, except r_{max}, shrink to zero and r_{max} assumes a stable radius. Thus, the model with tension-coupled pores does not predict membrane rupture and the predicted postshock growth of pores is consistent with experimental evidence.

DOI: 10.1103/PhysRevE.67.021915 PACS number(s): 87.16.Dg, 87.16.Ac, 87.50.Rr, 87.54.Dt

I. INTRODUCTION

Since late 1970s, the physical mechanism of the creation and evolution of pores has been described by the Smoluchowski equation (SE) [1–3],

$$n_t - D\frac{\partial}{\partial r}\left(\frac{E_r}{kT}n + n_r\right) = S(r). \tag{1}$$

In Eq. (1), the dependent variable is $n(r,t)$, the pore density distribution, such that at a given time t, the number of pores (per unit area) with radii between r and $r+dr$ is $n(r,t)dr$. D is the diffusion coefficient of the pore radius (5×10^{-14} m^2 s^{-1} [4]), $E(r)$ is the pore energy, k is the Boltzmann constant, and T is the absolute temperature (310 K, body temperature). $S(r)$ is a function representing creation and destruction of pores. It assumes that hydrophobic pores are created at a rate that depends exponentially on the square of the transmembrane potential (V) [5,6]. Pores with radii $r \geqslant r_*$ (Fig. 1, inset) convert spontaneously to long-lived hydrophilic pores. Resealing occurs when the pore radius decreases below r_*: the pore reverts to the hydrophobic configuration and is destroyed by lipid fluctuations [6]. The detailed mathematical description of $S(r)$ can be found in Ref. [7]; it is not important for the present study.

SE predicts that the pore radius, while subject to some thermal fluctuations, will expand or contract to minimize the pore energy (Fig. 1). For hydrophilic pores with $r \geqslant r_*$ and in the absence of an externally induced V, the pore energy is:

$$E(r) = \left(\frac{C}{r}\right)^4 + \gamma 2\pi r - \sigma_0 \pi r^2. \tag{2}$$

The three terms represent energy due to steric repulsion of lipid heads, line energy of the pore perimeter, and tension of the intact membrane [7]. In Eq. (2), C is the steric repulsion coefficient (from Ref. [7]), γ is the edge energy of the pore (1.8×10^{-11} J m^{-1} [4,6]), and σ_0 is the surface tension of the membrane (10^{-3} J m^{-2} [4]). Equation (2) and its illustration in Fig. 1 are based on the continuum representation of pore energetics, which is appropriate for large pores but is unlikely to remain valid as the size of the pore approaches the size of a lipid molecule.

The SE (1) has been used with success in theoretical studies of irreversible breakdown and rupture of the artificial lipid bilayers and biological cells [8,9], as well as in the studies of reversible electroporation with a large number of small pores [2,4]. However, it has problems with modeling large and long-lived pores. The pore energy of Fig. 1 predicts

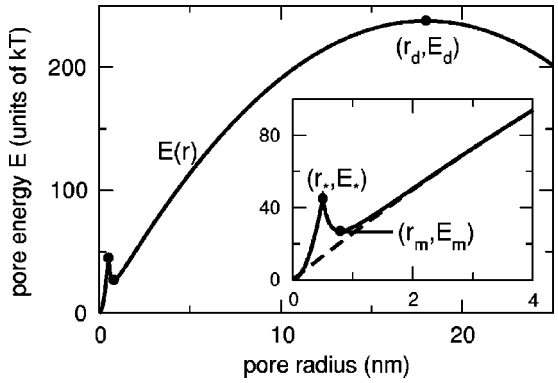

FIG. 1. (a) Energy E of a pore as a function of its radius at the transmembrane potential $V=0$. The radii r_* and r_d indicate positions of energy barriers for creation of hydrophilic pores and for rupture of the membrane, respectively; r_m is the position of a local energy minimum. Inset: full (solid line) and simplified (dashed line) pore energies.

*Corresponding author.
Electronic address: wanda. krassowska@duke.edu

two possible scenarios for the postshock evolution of pores created by a short electric pulse. After the pulse is turned off, pores with radii below r_d will shrink to the radius near the minimum energy radius $r_m \approx 0.8$ nm. Pores with radii above r_d will expand without bounds, leading to the irreversible breakdown and membrane rupture. Both processes happen very fast [4,9], so that measurements taken a few microseconds after the pulse should reveal either the presence of many pores with radii below 1 nm or the cell should be destroyed. However, experiments often document pores with diameters up to micrometers, which can persist without rupturing the membrane for tens of milliseconds to seconds [10,11]. Another feature not seen in the model is the postshock growth of pores and the stabilization of their radii at 20–60 nm [12]. To our knowledge, no in-depth explanation of this discrepancy between predictions of the SE and experimental results has been presented.

Our study addresses this problem by reexamining the energy cost of the creation and expansion of pores. The original formulation of the energy function (2) assumes that pores are independent: their energy depends only on their radii [Eq. (2)]. However, in reality pores are not independent: they are coupled through the tension of the membrane. The creation of many pores and/or their expansion relieves the membrane tension. As seen in Eq. (2), the decrease in σ_0 would increase the energy cost of creating new pores or expanding existing ones, potentially halting further growth of the pores.

A similar coupling between membrane tension and the pore area has been proposed before [11,13–15]. In these studies, the analysis was limited to either one giant pore, with the radius on the order of micrometers [11,15] or to a population of pores with identical radii [13]. Neither of these cases represents conditions occurring during electroporation-mediated drug or DNA delivery experiment. The present paper fills this gap.

When electroporation is used for drug or DNA delivery, the cells are exposed to an electric pulse, or a train of pulses, which creates a heterogeneous population of pores with radii ranging from zero to tens of nanometers. After the pulsation, the cells are usually allowed to reseal and are not subject to any additional manipulations. This is in contrast to several experimental studies [10,11,15], which used mechanical means to keep the membrane tension constant in order to elucidate the mechanisms of the pore evolution. However, this is an artificial situation: in practical applications, the change of pore radii following the pulsation is accompanied by the change in membrane tension. The present paper concentrates on the coupling of these two processes, so it focuses on the behavior of pores in cells that are ''left alone'' after pulsation, as it is usually done in drug and gene delivery applications.

The derivation of the theory of tension-coupled pores is presented here under two simplifying assumptions. First, in order to focus on the postshock evolution of large pores, this study will ignore the influence of the externally imposed potential V. Hence, the function $S(r)$ in SE (1) will be set equal to zero, since no creation of pores occurs in the absence of V and the resealing of pores takes much longer time (seconds) than the time scale considered here (microseconds to milliseconds). The process of creating pores by an external potential V will be represented by assuming an initial pore density distribution $n(r,t=0)$.

Second, since this study considers pores with very large radii, the steric repulsion of lipid heads is negligible and the first term of pore energy (2), $(C/r)^4$, does not have to be explicitly considered. This term creates an energy barrier at r_*, which slows down resealing of pores; in the simplified version, this barrier will be represented by a no-flux boundary condition at $r=0$. Approximation of r_* by zero follows from the scaling appropriate for large pores (introduced in Sec. III A), in which radii on the order of r_* are asymptotically equal to zero.

Under these assumptions, the SE (1) becomes

$$n_t - D\frac{\partial}{\partial r}\left(\frac{2\pi}{kT}(\gamma-\sigma_0 r)n + n_r\right) = 0, \tag{3}$$

where $2\pi(\gamma-\sigma_0 r)$ is the r derivative of the simplified pore energy. This energy is shown as a dashed line in the inset to Fig. 1. This figure demonstrates that the simplification affects only small radii and the energy of large pores is unchanged.

II. THEORY OF ELECTROPORATION WITH TENSION-COUPLED PORES

A. Energy of a bilayer and effective surface tension

Consider a lipid bilayer of area A, which consists of $2M$ lipid molecules. The interfacial energy per molecule, μ, is

$$\mu = \sigma' a + K/a, \tag{4}$$

where σ' is the interfacial energy per area of the hydrocarbon-water interface (20×10^{-3} J m^{-2} [16]), $a = A/M$ is the area per lipid head, and K is a constant [16]. The two terms in Eq. (4) give rise to attractive and repulsive forces, which balance at the optimal area per lipid head, $a_0 = \sqrt{K/\sigma'}$. Restating Eq. (4) in terms of a_0 yields

$$\mu = \sigma' a\left(1 + \frac{a_0^2}{a^2}\right). \tag{5}$$

The energy of the $2M$-molecule bilayer, W, is obtained as a sum of the energies of its molecules,

$$W = 2M\mu = 2\sigma' A\left(1 + \frac{A_0^2}{A^2}\right), \tag{6}$$

where $A_0 = Ma_0$ is the optimal area of the $2M$-molecule bilayer. For $A \geqslant A_0$, $\partial W/\partial A$ is positive and the membrane is under tension.

Expression (6) applies to an intact membrane. The presence of pores has a twofold effect: it decreases W by reducing the area subject to interfacial tension, and it increases W by introducing line energy of the pore perimeter. If A_p is the combined area of pores and L_p is the combined pore perimeter, then the bilayer energy is

$$W=\gamma L_p+2\sigma'(A-A_p)\left(1+\frac{A_0^2}{(A-A_p)^2}\right). \tag{7}$$

The above expression is the basis for estimating the effective surface tension of a bilayer, defined as the derivative of energy with respect to bilayer area A. In Eq. (7), regard A_p as an independent variable and A as a fixed constant. If the pore area changes by amount δA_p, the total bilayer area $A-A_p$ changes by amount $-\delta A_p$. Hence, the effective surface tension σ_{eff} is

$$\sigma_{eff}(A_p)=-\frac{\partial W}{\partial A_p}=2\sigma'\left(1-\frac{A_0^2}{(A-A_p)^2}\right)$$

$$=2\sigma'-\frac{2\sigma'-\sigma_0}{(1-A_p/A)^2}. \tag{8}$$

In Eq. (8), σ_0 denotes the surface tension of the intact membrane with $A_p=0$,

$$\sigma_0=2\sigma'\left(1-\frac{A_0^2}{A^2}\right). \tag{9}$$

A value of σ_0 used in the literature, 1 mJ m^{-2}, requires only a small fractional change in membrane area: $(1-A_0/A)=0.0126$.

Returning to the energy of a bilayer: using definition of σ_0 (9), Eq. (7) can be rewritten as

$$W=\gamma L_p+2\sigma'(A-A_p)+(2\sigma'-\sigma_0)\frac{A^2}{A-A_p}. \tag{10}$$

This energy can be normalized by subtracting the energy of the intact membrane, so that W is zero for $A_p=0$,

$$W=\gamma L_p-\left(2\sigma'-\frac{2\sigma'-\sigma_0}{1-A_p/A}\right)A_p. \tag{11}$$

B. Mean field theory of pore statistics

Each pore in the entire population ''feels'' the effective surface tension σ_{eff} in place of σ_0. This observation motivates a heuristic description of pore statistics: The pore population is still described by an equation like the Smoluchowski equation (3) but the constant surface tension σ_0 is replaced by σ_{eff}:

$$n_t-D\frac{\partial}{\partial r}\left(\frac{2\pi}{kT}[\gamma-\sigma_{eff}(A_p)r]n+n_r\right)=0. \tag{12}$$

In Eq. (12), the effective tension σ_{eff} depends on A_p, which in turn depends on the pore density distribution $n(r,t)$:

$$A_p=A\int_0^\infty \pi r^2 n(r,t)dr. \tag{13}$$

Due to the functional dependence of σ_{eff} upon $n(r,t)$, Eq. (12) is a nonlinear integro-differential equation (NIDE) for $n(r,t)$.

As stated in the Introduction, there is a no-flux boundary condition at $r=0$, which means that loss of pores due to resealing is negligible. From Eq. (12), the rate of change of total pore number is

$$\frac{\partial}{\partial t}\left(A\int_0^\infty n(r,t)dr\right)=-Af(0,t), \tag{14}$$

where

$$f(r,t)\equiv -D\left(\frac{2\pi}{kT}[\gamma-\sigma_{eff}(A_p)r]n+n_r\right) \tag{15}$$

is the flux associated with the NIDE (12). The no-flux boundary condition is therefore

$$f(0,t)=0. \tag{16}$$

The description of pore statistics (12), (8) is a heuristically formulated mean field theory, analogous to other classical mean field theories, such as the Debye-Hückel theory of electrolytes [17]. In the Appendix, the thermodynamic free energy of a bilayer with tension-coupled pores is formulated as a functional of n, and it is shown that this free energy decreases in time for $n(r,t)$ that satisfy the NIDE (12).

C. Special case: Homogeneous population of tension-coupled pores

A homogeneous population of pores, all with the same radius, is not likely to appear in practice. Nevertheless, it serves as an intuitive illustration of the formula for the bilayer energy (11) and as a preliminary analysis leading to the simplified equations governing the evolution of pores.

For a homogeneous population of pores, the pore density distribution $n(r,t)$ is

$$n(r,t)=N\delta(r-r_0), \tag{17}$$

where δ is the Dirac's function, $r_0=r_0(t)$ is the radius of pores, and $N\equiv\int_0^\infty n(r,t)dr$ is pore density. The area of pores is evaluated from Eq. (13),

$$A_p=A\pi N r_0^2, \tag{18}$$

and the effective surface tension is computed from (8) as

$$\sigma_{eff}=2\sigma'-\frac{2\sigma'-\sigma_0}{(1-\pi N r_0^2)^2}. \tag{19}$$

The energy of the bilayer with the homogeneous pores can be computed from Eq. (11). Evaluating the combined perimeter of pores,

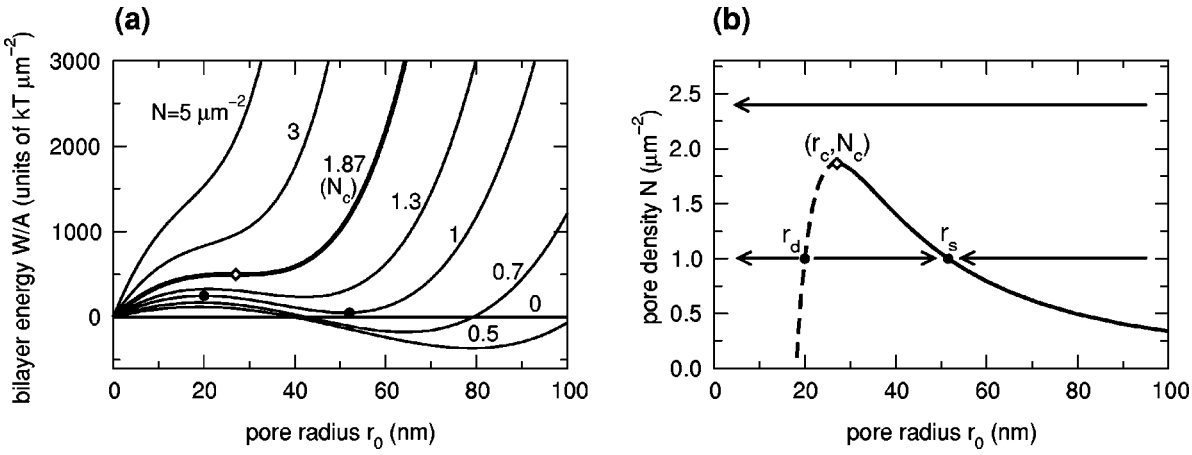

FIG. 2. Homogeneous population of pores. (a) Bilayer energy per area as a function of pore radius r_0. Values of N are indicated by labels. (b) Diagram showing regions of growth (right arrow) and shrinkage (left arrows) of pores as a function of initial radius r_0 and pore density N. N_c is the critical pore density, r_c is the inflection point (diamond), r_d is the position of the barrier for the spontaneous expansion of pores, and r_s is the stable radius. To obtain the diagram in (b), maxima and minima of quartic curves [shown in (a) as filled circles on $N=1\ \mu\mathrm{m}^{-2}$ plot] were computed by differentiating the right-hand side of Eq. (22), setting it to zero, and solving the resulting third-order equation.

$$L_p = A\int_0^\infty 2\pi r n(r,t)\,dr = A2\pi N r_0, \tag{20}$$

the bilayer energy per area takes the form

$$\frac{W}{A} = 2\pi\gamma N r_0 - \left(2\sigma' - \frac{2\sigma' - \sigma_0}{1-\pi N r_0^2}\right)\pi N r_0^2. \tag{21}$$

Expanding $1/(1-\pi N r_0^2)$ in Taylor's series, the bilayer energy becomes a quartic polynomial in r_0,

$$\frac{W}{A} \approx 2\pi\gamma N r_0 - \pi\sigma_0 N r_0^2 + (2\sigma' - \sigma_0)(\pi N)^2 r_0^4, \tag{22}$$

in which linear and quartic terms are positive, so they cause shrinking of pores, and the quadratic term is negative, so it causes expansion of pores.

Figure 2(a) shows the bilayer energy (22) as a function of r_0 for several values of pore density N. This figure suggests two different scenarios. When the electric shock creates a sufficiently large number of pores ($N>N_c$), W is a monotonically increasing function of r_0. Physically, it means that so many pores are created that not enough tension is left in the membrane to cause pore expansion. Hence, all pores will shrink to zero. When the electric shock creates a small number of pores ($N<N_c$), W has two energy minima, at zero and at r_s, separated by an energy barrier at r_d. Hence, small pores, with initial radius $r_0<r_d$, will shrink to zero and large pores, with initial radius $r_0>r_d$, will either expand or shrink until they achieve radius r_s. This radius is stable: once the pores reach r_s, their size remains unchanged until some external event, such as the change in cell volume through leakage, disturbs the equilibrium. These two cases are separated by the ''critical'' pore density

$$N_c = \frac{2}{27\pi}\frac{\sigma_0^3}{(2\sigma' - \sigma_0)\gamma^2} \approx 1.87\ \ \mu\mathrm{m}^{-2}, \tag{23}$$

for which W has a horizontal inflexion point at radius

$$r_c = \frac{3}{2}\frac{\gamma}{\sigma_0} \approx 27\ \ \mathrm{nm}. \tag{24}$$

The diagram in Fig. 2(b) summarizes the different scenarios described above. The positions of the maximum (r_d) and the minimum (r_s) of W, plotted on the (r_0,N) plane, show all combinations of the initial radius r_0 and pore density N that result in shrinkage of pores to zero (left of r_d curve or above N_c) versus setting down to a stable radius r_s (right of r_d curve).

The actual process of shrinkage or growth of pores in a heterogeneous population is governed by the NIDE (12), which can be solved numerically, but at a fairly large computational cost. For example, to obtain accurate numerical solutions to the SE (1), Joshi and Schoenbach used spatial and temporal discretization steps of 5 pm and 1 ps, respectively [9]. Our study uses an alternative approach: an asymptotic analysis of the NIDE shows that it can be reduced to ordinary differential equations (ODEs). The following section presents a derivation of these ODEs for an arbitrary population of pores and afterwards we will finish the example of a homogeneous pore population.

III. EVOLUTION OF PORES

A. Approximate solution of the mean field equation (12)

The first step in the analysis is converting NIDE (12) to dimensionless form using the following system of units:

Variable:	r	t	n	σ_{eff}	W/A
Unit:	r_c	$\frac{3}{4\pi}\frac{kT}{D\sigma_0}$	$\frac{N_c}{r_c}$	σ_0	$\gamma N_c r_c$
Value:	27 nm	20.4 μs	69.2 μm^{-3}	10^{-3} J m^{-2}	212 $kT\mu$m^{-2}.

(25)

The dimensionless form of NIDE (12) is

$$n_t - \frac{\partial}{\partial r}\left[\left(1-\frac{3}{2}\sigma_{eff}(A_p)r\right)n+\varepsilon n_r\right]=0, \tag{26}$$

where A_p and σ_{eff} are dimensionless counterparts of quantities defined by Eq. (13) and Eq. (8), respectively. The parameter ε appearing in Eq. (26) is defined as

$$\varepsilon=\frac{kT}{3\pi}\frac{\sigma_0}{\gamma^2}. \tag{27}$$

For typical values of σ_0, γ, and at the body temperature, ε has a small value of approximately 0.0015. This indicates that the diffusion term in Eq. (26) is at least two orders of magnitude smaller than others and can be neglected. Hence, NIDE (26) reduces to a first-order equation,

$$n_t - \frac{\partial}{\partial r}\left[\left(1-\frac{3}{2}\sigma_{eff}(A_p)r\right)n\right]=0. \tag{28}$$

This equation can be further transformed using the method of characteristics [18]. This procedure leads to ODEs governing the time evolution of pore radii and pore density distribution. Specifically, the radius r_i of the ith pore in the whole population of pores evolves according to the ODE:

$$\frac{dr_i}{dt}=-\left(1-\frac{3}{2}\sigma_{eff}(A_p)r_i\right). \tag{29}$$

The value of the pore density distribution, which is seen at time t and radius r_i, is denoted by $n_i(t)=n(r_i(t),t)$ and evolves according to the ODE:

$$\frac{dn_i}{dt}=-\frac{3}{2}\sigma_{eff}(A_p)n_i. \tag{30}$$

Returning to dimensional variables, Eqs. (29) and (30) take the form

$$\frac{dr_i}{dt}=-\frac{2\pi D}{kT}[\gamma-\sigma_{eff}(A_p)r_i], \tag{31}$$

$$\frac{dn_i}{dt}=-\frac{2\pi D}{kT}\sigma_{eff}(A_p)n_i, \tag{32}$$

where σ_{eff} is given by Eq. (8). Note that σ_{eff} is a function of time through its dependence on A_p and, consequently, on $n(r,t)$. This dependence can be incorporated in calculations as follows. Let us assume that known initial pore density distribution $n(r,0)$ is specified on a finite interval $r_{min}\leqslant r \leqslant r_{max}$. This interval is divided into K subintervals and $n(r,0)$ represented by pairs $r_i(0),n_i(0)$, $i=1,2,\ldots,K+1$. Thus, A_p at $t=0$ is evaluated using the trapezoidal rule [19], and σ_{eff} at $t=0$ is computed from Eq. (8). Now, r_i and n_i are advanced in time by solving $K+1$ pairs of ODEs, Eqs. (31) and (32). Using new r_i and n_i, σ_{eff} can be updated and the process repeated in each time step.

Solutions to Eqs. (31) and (32) can be obtained using standard numerical techniques. This paper uses an implicit midpoint method with Newton-Ralphson iteration in each time step [19]. The time step needed for a convergent and accurate solution is only 0.1 μs, which is five orders of magnitude larger than the time step used for the direct solution of the Smoluchowski equation in [9].

B. Special case: Homogeneous population of tension-coupled pores

Applying the results of Sec. III A to a homogeneous population of pores, $n(r,t)=N\delta(r-r_0)$, gives an ODE governing the time evolution of the radius of all pores $r_0(t)$,

$$\frac{dr_0}{dt}=-\frac{2\pi D}{kT}[\gamma-\sigma_{eff}(r_0,N)r_0], \tag{33}$$

where $\sigma_{eff}(r_0,N)$ is given by Eq. (19).

Figure 3 illustrates the time evolution of pores for three values of pore density N and three initial radii. In agreement with predictions of the bilayer energy of Fig. 2(a) and the diagram of Fig. 2(b), $N>N_c$ always results in pores shrinking to zero, while $N<N_c$ may lead either to shrinkage to zero

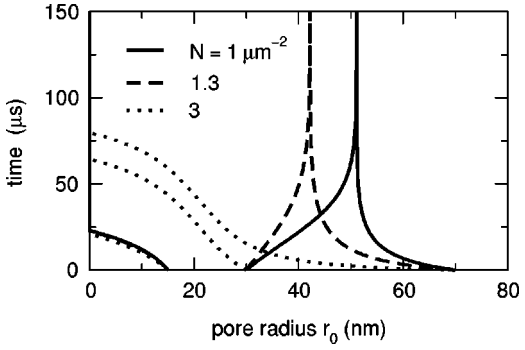

FIG. 3. Homogeneous population of pores, time evolution of pore radius $r_0(t)$. Solid, dashed, and dotted lines correspond to three pore densities (legend): $N=1$ and 1.3 μm^{-2} (below N_c), and 3 μm^{-2} (above N_c). Each pore density was tested for three initial radii: $r_0(0)=$ 15 nm (below r_c), and 30 and 70 nm (above r_c).

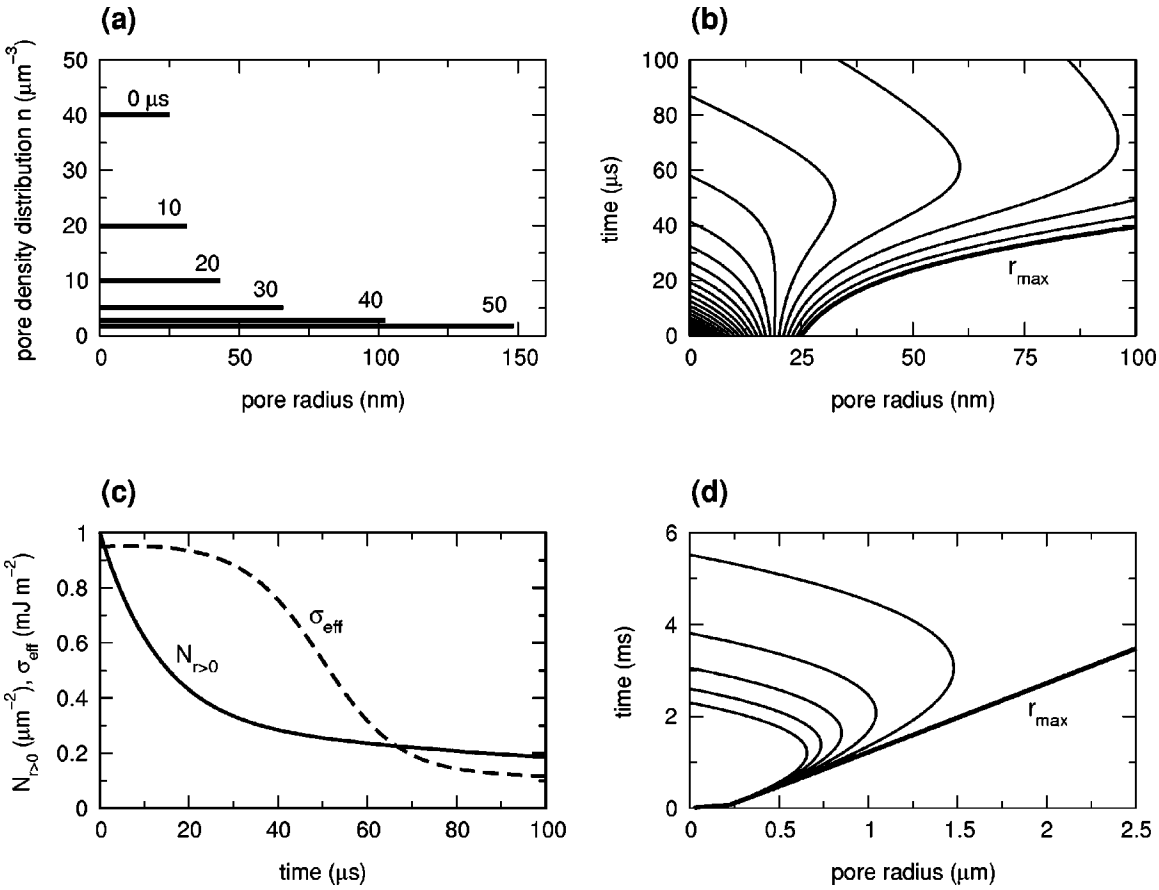

FIG. 4. Heterogeneous population of pores, time evolution of a uniform distribution with initial radii $0 \leqslant r(0) \leqslant 25$ nm and pore density $N=1\ \mu\mathrm{m}^{-2}$. (a) Pore density distribution $n(r,t)$ plotted as a function of radius r at six instants of time, $t=0,10,\ldots,50\ \mu$s. (b) Time evolution of 25 representative radii, $r_i(0)=1,2,\ldots,25$ nm. (c) The density of pores with nonzero radii $N_{r>0}$ (solid line) and the effective membrane tension σ_{eff} (dashed line) plotted as a function of time. (d) Time evolution of six large radii, $r_i(0)=24.9,24.92,\ldots,25$ nm, followed for longer time interval, $0 \leqslant t \leqslant 6$ ms.

or to stabilization of pores at radius r_s. The time scale of this process is on the order of microseconds, as is the time unit used for scaling (25).

IV. EXAMPLE: UNIFORM DISTRIBUTION OF PORES

A. Continuum formulation

A homogeneous population of pores, analyzed above, may not appear in real-life situations. Hence, the next example recognizes that the shock creates a heterogeneous population of pores, with radii ranging from zero to some value r_{max}. For simplicity, the pore density distribution at time $t=0$ is assumed uniform,

$$n(r,0)=\begin{cases} N/r_{max}, & 0 \leqslant r \leqslant r_{max} \\ 0, & r > r_{max}, \end{cases} \tag{34}$$

where N is the pore density. This distribution is represented by pairs $r_i(0), n_i(0)$, $i=1,2,\ldots,K+1$, where $K+1$ is chosen so that at $t=0$, adjacent radii are separated by at least 0.1 nm. The time evolution of pairs $r_i(t), n_i(t)$ is computed from ODEs (31) (32), with A_p evaluated numerically from Eq. (13) and σ_{eff} from Eq. (8).

Figure 4 illustrates a typical time evolution of a uniform distribution of pores. This example assumes $r_{max}=25$ nm and $N=1\ \mu\mathrm{m}^{-2}$. As seen in Fig. 4(a), $n(r,t)$ remains uniform in r at all times. This is a consequence of advection velocity in NIDE (12) being a linear function of r. With the linear velocity, the distribution will change its range and magnitude, but it will retain its original shape. Figure 4(b) shows the evolution of 25 representative pores. Pores with $r_i(0)<20$ nm shrink from the very onset of the simulation. As the radii of these pores become zero,[1] the density of pores with nonzero radius, $N_{r>0}$, steadily decreases [Fig. 4(c), solid line] and less pores are available to relieve membrane tension. However, the growth of larger pores compensates for the decrease in $N_{r>0}$ and σ_{eff} decreases [Fig. 4(c), dashed line]. This is an example of a general phenomenon, the ''coarsening'' [20], which has been observed in other physical systems such as solid crystals nucleating from liquid solution.

The long-time behavior of the uniform pore distribution is shown in Fig. 4(d), which follows evolution of six very large

[1]More precisely, pore radii become $O(\varepsilon)$, so that the no-flux boundary condition at $r=0$ is preserved (see Sec. V B).

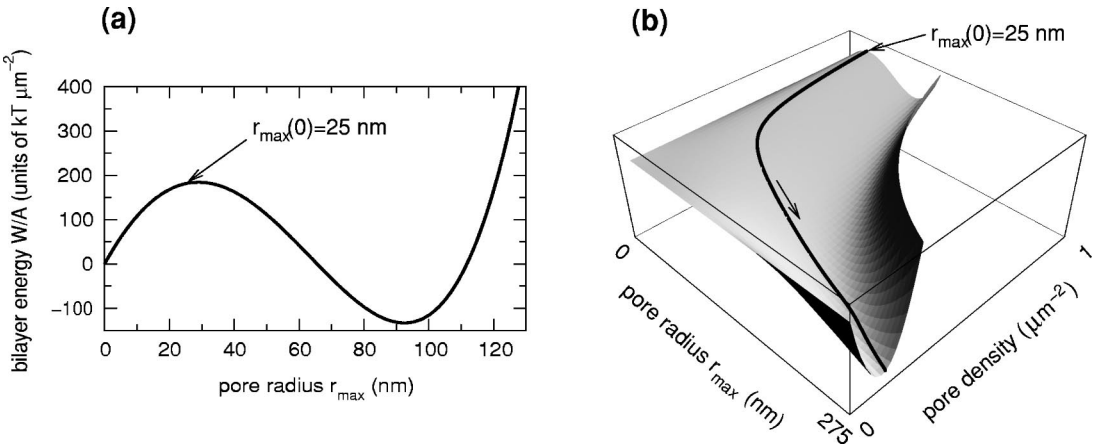

FIG. 5. (a) Bilayer energy per area plotted as a function of the maximum radius r_{max} of the uniform distribution. Pore density $N=1\ \mu\mathrm{m}^{-2}$. (b) Bilayer energy per area plotted as a function of the maximum radius r_{max} and the pore density N. The line shows the trajectory $r_{max}(t)$ that starts at 25 nm.

pores, with initial radii from 24.9 to 25 nm. This figure shows that all pores with radii $r<r_{max}$ eventually shrink to zero. This result can be intuitively explained as follows. Because smaller pores keep shrinking to zero and the distribution must remain uniform, coarsening continues: even larger pores, which initially grow, must eventually turn around and start shrinking. This is the ultimate fate of all pores except r_{max}, which must continue to grow, in order to prevent the increase in membrane tension. Asymptotically, the growth of r_{max} becomes linear, with the slope $dr_{max}/dt\rightarrow\pi\gamma D/kT$ as $t\rightarrow\infty$.

The scenario illustrated in Fig. 4 is qualitatively different from the behavior of the homogeneous pore population (Fig. 3). The most important difference is the absence of stable pores with radii of tens of nanometers. Based on the bilayer energy plotted as a function of r_{max} [Fig. 5(a)], one would expect r_{max} to reach the stable radius corresponding to the energy minimum. However, one must take into account that as r_{max} moves towards this minimum-energy radius, the smallest pores shrink to zero [Fig. 4(b)] and the pore density N effectively changes [Fig. 4(c)]. Hence, in the case of a heterogeneous pore distribution, the bilayer energy W must be considered a functions of both r_{max} and N. Figure 5(b) shows this function as a surface in the three-dimensional space: note that the energy minimum at $t=0$, shown in Fig. 5(a), is a part of a ''valley'' that becomes deeper as $N\rightarrow 0$ and $r_{max}\rightarrow\infty$. The trajectory overlaid on this surface shows that $r_{max}(t)$ eventually follows the bottom of this valley, minimizing the bilayer energy.

Once one accepts the correctness of the results shown in Fig. 4, the implication is that the model with tension-coupled pores cannot predict large and stable pores. Contrary to the results for a homogeneous pore population (Fig. 3), in a more general case of a heterogeneous pore population, the relief of membrane tension by pores does not prevent the largest pore from unbounded growth and rupturing the membrane.

This conclusion is too hasty because it does not take into account the limitations of the continuum approximation. Let us consider a cell of radius 10 μm. In the example shown in Fig. 4, the initial pore density, $N=1\ \mu\mathrm{m}^{-2}$, corresponds to 1256 pores per cell. However, for the final time shown in Fig. 4(d), 6 ms, $N=0.7\times10^{-3}\ \mu\mathrm{m}^{-2}$, which corresponds to only 0.89 pores. For a fractional number of pores per cell, the behavior of the continuum model no longer reflects reality. Hence, the following section will reexamine the same problem using a discrete formulation.

B. Discrete formulation

Let us consider a heterogeneous population of pores with the initial pore density N. For a spherical cell of radius R, the number of pores is

$$K=A_{cell}N=4\pi R^2N. \tag{35}$$

This example assumes that at $t=0$ pore radii are distributed uniformly between zero and r_{max},

$$r_i=ir_{max}/K,\quad i=1,2,\ldots,K. \tag{36}$$

The time evolution of each radius r_i is governed by the ODE (31). Effective tension σ_{eff} is computed from Eq. (8) and the bilayer energy W is computed from Eq. (11). In these expressions, A_p and L_p are computed by summing areas and circumferences of all pores,

$$A_p=\sum_{i=1}^{K}\pi r_i^2,\quad L_p=\sum_{i=1}^{K}2\pi r_i, \tag{37}$$

and A is the cell area A_{cell} computed as in Eq. (35).

Figure 6 is the counterpart of Fig. 4(d) for the discrete model. The pore density $N=1\ \mu\mathrm{m}^{-2}$, and the initial radii of the six pores, 24.9 to 25 nm, are the same as shown in Fig. 4(d). At $t=0$, a cell of radius $R=10\ \mu$m is assumed to have 1256 uniformly distributed pores; the figure shows the time evolution of the six largest pores, 1251–1256. Five of these pores, with radii $r<r_{max}$, shrink to zero; smaller pores (not shown) shrink even faster, just as they did in the continuum model. However, the largest pore, r_{max}, grows to a stable radius r_s. Note the time scale of the process: it takes almost

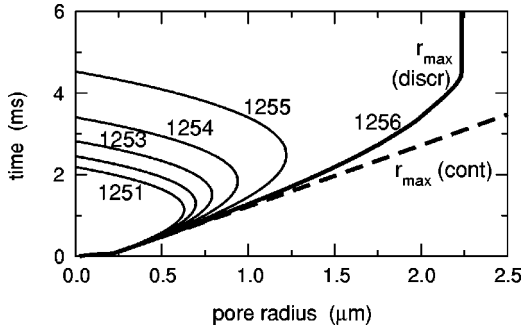

FIG. 6. Time evolution of a uniform distribution of pores in a discrete model. At time $t=0$, there are 1256 pores with radii $0<r_i(0)\leqslant 25$ nm. Shown here is the time evolution of the six largest pores, $r_i(0)=24.9,24.92,\ldots,25$ nm (solid lines); the same as in Fig. 4(d). The heavy line shows the evolution of r_{max} of the discrete model; the dashed line shows the evolution of r_{max} of the continuum model [from Fig. 4(d)].

4.5 ms for r_{max} to reach its stable radius. Also note the large final size of r_s, 2.234 μm, which is over 20% of cell radius. The same value is obtained by computing from Eq. (11) the position of the bilayer energy minimum. Note that at r_s, the tension of the membrane is not zero: $\sigma_{eff}=8.1\times10^{-6}$ J m^{-2}, or 0.81% of σ_0. This small σ_{eff} is needed to balance the force exerted by line energy.

The reason why the largest pore in the discrete model settles at a stable radius is illustrated in Fig. 7. This figure shows the bilayer energy as a function of r_{max} and N [continuum model, Fig. 7(a)] and r_{max} and K [discrete model, Fig. 7(b)]. These two surfaces are drawn for the case when there are very few pores per cell: K varies between 1 and 12. In the continuum case, N can assume any real number, so the energy surface is smooth. In the discrete case, K assumes only integer values, so the energy surface decreases in clearly visible steps. There also is a natural termination of the discrete energy surface at $K=1$. When K decreases to zero, the last pore disappears and the energy sharply increases to a value corresponding to that of an intact membrane. There is no such natural termination in a continuum model, so r_{max} can increase without bounds. However, the increase of r_{max} predicted by the continuum model has no physical significance.

V. DISCUSSION

A. Difference between the Smoluchowski equation (3) and the mean field equation (12)

This study proposes a model in which the behaviors of individual pores are not independent: the pores are coupled by the tension of the membrane. This model can be considered a nonlinear extension of the Smoluchowski equation used in the literature to describe the behavior of uncoupled pores [1–3]. The purpose of this part of the discussion is to preempt misunderstandings invited by formal resemblance of NIDE (12) to SE (3).

First, consider the ensemble of uncoupled pores with the single pore energy

$$E(r)=2\pi\gamma r-\pi\sigma_0 r^2. \tag{38}$$

The internal energy of this system (''bilayer energy'') is the combined energy of all pores:

$$W_0=A\int_0^\infty E(r)n\,dr=\gamma L_p-\sigma_0 A_p. \tag{39}$$

Now consider the system of tension-coupled pores. Its internal energy is equal to the bilayer energy W defined by Eq. (11). Note that W in Eq. (11) is not equal to W_0 in Eq. (39) with σ_0 replaced by σ_{eff} because the expression in parentheses is not equal to σ_{eff} defined by Eq. (8): in Eq. (8), term $(1-A_p/A)$ is squared. This difference arises from the fact that as pores are successively created, their energy cost de-

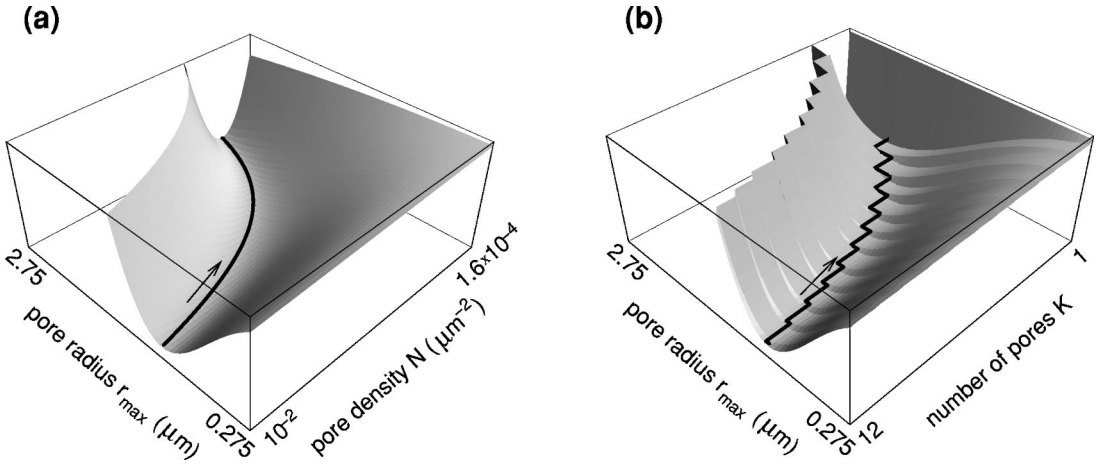

FIG. 7. Bilayer energy per area of a continuum and a discrete model. Shown are parts of the energy surface that correspond to a small number of pores per cell. (a) Continuum model: the energy is plotted as a function of the maximum radius r_{max} and the pore density N. (b) Discrete model: the energy is plotted as a function of the maximum radius r_{max} and the number of pores K. Lines indicate trajectories $r_{max}(t)$ that start at 25 nm, arrows indicate the direction of movement. Note the opposite orientation of these plots from the surface shown in Fig. 5(b).

pends on previously created pores. Thus, in a system with tension-coupled pores, the internal energy W is not the sum of individual pore energies.

B. Simplifying assumptions and future work

The model presented here contains several simplifying assumptions. First, the model simplifies the shape of the pore energy function (Fig. 1, inset) by neglecting the contribution of steric repulsion. Consequently, in the model pores shrink to zero radius, while in reality they accumulate at the radius of ≈ 0.8 nm, which corresponds to the local energy minimum. This simplification is of no consequence; the same qualitative results will be obtained if the bilayer energy includes the steric repulsion term. The presence of 0.8 nm radius pores has only a small effect on membrane tension, so the quantitative effect on the result is expected to be negligible.

Likewise, simplifying NIDE (12) to ODEs for the purpose of obtaining numerical solution is of no practical consequence. This simplification neglects the thermally induced diffusion of pore radii, which would result in a slight modification of the pore density function $n(r,t)$. The length scale of the diffusion, $L_D \propto \sqrt{DT_D}$, where D is the diffusion coefficient and T_D is the relevant time scale [21]. Using the time unit from scaling table (25) as T_D, $L_D \approx 1$ nm, which is much smaller than 27 nm, the length scale from table (25). Hence, the diffusion is expected to introduce only a small quantitative change for $r \gg 1$ nm. For example, in the uniform distribution of Fig. 4(a), sharp edge at r_{max} would be blurred.

However, neglecting diffusion creates an appearance of inconsistency in the model: the number of finite-size ($r > 0$) pores decreasing with time [Fig. 4(c)] conflicts with the no-flux boundary condition (16) at $r=0$, which ensures the conservation of pores. This is an artifact of the reduced NIDE (28), which is not sufficient to resolve a boundary layer of thickness ε at $r=0$, where diffusion matters. Given a solution $n(r,t)$ of the reduced equation (28), a uniformly valid approximation to a solution of the full NIDE (26) is given by

$$n_{full} \approx \frac{N_0(t)}{\varepsilon} e^{-r/\varepsilon} + n(r,t). \tag{40}$$

Here, $N_0(t)$ is a function of time, independent of r. The first term on the right-hand side dominates for r of magnitude ε, and represents a high density of pores whose radii have collapsed to magnitude ε. Based on Eq. (40), the approximation to the total pore density is

$$N \approx N_0 + N_{r>0}, \tag{41}$$

where $N_{r>0} \equiv \int_0^\infty n(r,t)dr$ can be thought of as the density of pores with $r \gg \varepsilon$ and N_0 as the density of pores with $r = O(\varepsilon)$. Given $N_{r>0}$ from a solution of reduced equation (28), $N_0 = N - N_{r>0}$. The actual structure of the boundary layer at $r=0$ is not important, since NIDE (26) is already based on a simplified pore energy valid only for pores significantly larger than 1 nm and, moreover, the continuum representation of pore energy has limited validity for small pores. The main point is that there is a large concentration of pores that have collapsed to a radius $r = O(\varepsilon)$ and the pore conservation is upheld. However, as mentioned above, pores that small have negligible influence on membrane tension and can be ignored.

The coarsening process studied here is driven by changes in membrane tension induced by replacing the lipid bilayer by water-filled pores. An alternative mechanism of the coarsening process is the decrease in line energy caused by the coalescence of the adjacent pores [22]. This mechanism is not included in the present model because of the relatively low pore densities considered here: the initial $N = 1\ \mu\text{m}^2$ corresponds to the interpore distance of approximately $1\ \mu$m, which is much larger than the initial pore radii, 0–25 nm. Since the number of pores decreases with time (Fig. 4), the coalescence of adjacent pores would be rare and would have only a small effect on the results.

Neglecting the effect of the transmembrane potential V is of more consequence. The examples presented here assume arbitrary and idealized initial distributions of pore density $n(r,0)$ and concentrate on the postshock evolution. This was done to maintain the clarity of presentation. The processes related to potential V, such as charging the membrane by an external electric shock and the creation of pores, proceed with similar time constants as the evolution of pore radii. With all these processes happening at the same time, the problem becomes intrinsically ''messy.'' Nevertheless, the problem in which creation and evolution of pores are coupled to V is of practical interest and will be addressed in future work.

Another unphysiological assumption is that the volume of the cell remains constant. In reality, creation of pores of the size investigated here leads to the leakage of cellular content. This process aids in the decrease of membrane tension, possibly modifying later stages of pore evolution. Thus, another extension of the present model should be the addition of changes in cell volume. The coupling of the pore evolution with the change of cell volume has been proposed before, although in the case of only one pore present [11,15].

C. Comparison with experimental results

Numerical simulations of the original Smoluchowski equation (1) reveal that pores increase their radius very rapidly when the electric shock is present. As soon as the shock is turned off, pores either shrink to zero or, if pores with radii above 20 nm have been created, they expand without bounds, leading to the rupture of the membrane [4,9]. The predicted time scale of these processes is on the order of a fraction of a microsecond. Postshock growth of pores to radii on the order of tens of nanometers, lasting for milliseconds and followed by their shrinkage and resealing, has not been seen in simulations.

Thus, the original SE cannot explain the study of Chang and Reese, who used rapid-freezing electron microscopy to visualize the evolution of pores in red blood cells [12]. The resolution of the method allowed the pores to be first seen approximately 3 ms after the shock, when their radii were

10–20 nm. The pores continued to grow, and their radii stabilized 40 ms after the shock at 20–60 nm. The resealing of pores started at 5 s.

These experimental results have several common features with the predictions of our model of tension-coupled pores. The model predicts the postshock growth of pores, the time scale is on the order of milliseconds, the pore radii are tens of nanometers and larger, and the membrane does not rupture (Fig. 6). However, the simplifications of our model introduce several quantitative differences. First, the pore radii stabilize after 4 ms in the model (Fig. 6), and after 40 ms in the experiment. This difference is most likely due to model parameters corresponding roughly to planar lipid bilayers, not to red blood cells. It is also possible that the later growth of pores was caused by the swelling of cells, which is not represented in the model. Second, Chang and Reese did not see a coarsening process leading to the presence of only one pore. This difference can be explained by the existence of a network of cytoskeletal proteins in red blood cells. The tension coupling between pores would be limited only to pores in the same opening of the network, so the coarsening process would lead to one pore per opening, instead of one pore per cell. Finally, the largest pore observed in the model, 2.234 μm, is larger than the pores in the experiment, 60 nm. This difference is easily explained: since many pores contribute to the relieving membrane tension, the radii of the individual pores can be smaller. Smaller radii were predicted by the model for the homogeneous distribution of pores (Figs. 2 and 3).

To see that the coarsening process indeed leads to one pore, one needs to examine experiments performed on liposome vesicles, which do not have cytoskeletal networks. Such liposomes, 25–50 μm in diameter, were used in a study of Zhelev and Needham [10]. Pores were induced by a 150 μs, 0.63–1.26 kV cm^{-1} electric shock. Based on a study of Hibino *et al.* [23], such a shock should create a large number of pores, concentrated in the parts of the liposome membrane facing the electrodes. Yet, when the liposome was examined several milliseconds after the shock, only one pore, with the radius of approximately 1 μm, was present. Hence, this experiment indicates that the coarsening process predicted by the model (Fig. 6) may be taking place.

Another confirmation comes from the experiment of Sandre *et al.*, performed on stretched liposome vesicles [11]. In this study, the viscosity of the solvent was increased in order to slow down the rate of leakage from the cell. Hence, in the slow leakage limit, this experiment approximates the constant cell volume situation assumed by our model. Images collected several times per second revealed the presence of only one pore. Sandre *et al.* observed the stabilization of this pore at a radius up to 10 μm; afterwards, the leakage through the pore took over and led to the decrease of cell volume, shrinkage of the pore, and its resealing. These comparisons between theory and experiments give us a reason to believe that, despite its simplifying assumption, the model with tension-coupled pores can be useful in theoretical studies of the postshock evolution of pores.

ACKNOWLEDGMENTS

Part of this work was done during W. Krassowska's sabbatical at Genetronics, Inc., San Diego, CA. This work was supported in part by the National Science Foundation Grant Nos. BES-9974185 and BES-0108408.

APPENDIX: MEAN FIELD THEORY AND FREE ENERGY OF TENSION-COUPLED PORES

The purpose of this appendix is to make a connection between the energetics of the system of tension-coupled pores and the mean field NIDE (12). In particular, it will be shown that the free energy

$$F = W - TS, \tag{A1}$$

with the internal energy W as in Eq. (7), is nonincreasing in time for $n(r,t)$ that satisfy the NIDE (12). The association of a free energy with the kinetics of a mean field theory was first worked out by Bonilla *et al.* [24].

The argument uses the dimensionless quantities, expressed in units from the scaling table (25). Also, in this appendix, F, W, and S represent energies and entropy per area, rather than those of the entire bilayer. Hence, the dimensionless free energy per area is

$$F = W - \varepsilon S, \tag{A2}$$

where S is the dimensionless entropy per area,

$$S = -2\pi \int_0^\infty n \ln(n) dr. \tag{A3}$$

The small parameter ε, defined in Eq. (27), is proportional to temperature, so Eq. (A2) amounts to the standard definition of free energy in thermodynamics [25]. The internal energy W is evaluated as follows. From Eq. (7), the bilayer energy per area can be written as

$$W = \gamma \frac{L_p}{A} + 2\sigma' \frac{A - A_p}{A} \left(1 + \frac{A_0^2}{(A - A_p)^2} \right). \tag{A4}$$

Hence, the dimensionless internal energy is

$$W = \int_0^\infty 2\pi r n dr + \frac{1}{\gamma N_c r_c A} \left[2\sigma' (A - A_p) \times \left(1 + \frac{A_0^2}{(A - A_p)^2} \right) \right], \tag{A5}$$

where dimensionless A, A_0, and A_p are measured in units of r_c^2.

Now compute the time rate of change of F,

$$\dot{F} = \dot{W} - \varepsilon \dot{S}, \tag{A6}$$

where $\dot{W}$ and $\dot{S}$ are obtained by differentiating W and S in (A5) and (A3), respectively. First compute

$$\dot{W}=\int_0^\infty 2\pi r n_t dr+\frac{1}{\gamma N_c r_c A}\frac{\partial}{\partial A_p}\left[2\sigma'(A-A_p)\times\left(1+\frac{A_0^2}{(A-A_p)^2}\right)\right]\frac{\partial A_p}{\partial t}$$
$$=2\pi\int_0^\infty\left[r-\frac{3}{4}\sigma_{eff}(A_p)r^2\right]n_t dr, \tag{A7}$$

where the derivative $\partial/\partial A_p$ of the expression in brackets is recognized as equal to dimensionless σ_{eff} times $(-\sigma_0)$. Next, from Eq. (A3),

$$\dot{S}=-2\pi\int_0^\infty[\ln(n)+1]n_t dr=-2\pi\int_0^\infty\ln(n)n_t dr. \tag{A8}$$

The last equality in Eq. (A8) is due to effective conservation of pores,

$$\frac{d}{dt}\int_0^\infty n dr=0, \tag{A9}$$

which ignores the possibility of the pore coalescence. With the above results for $\dot{W}$ and $\dot{S}$, the rate of change of free energy in Eq. (A6) becomes

$$\dot{F}=2\pi\int_0^\infty\left(r-\frac{3}{4}\sigma_{eff}(A_p)r^2+\varepsilon\ln(n)\right)n_t dr$$
$$=-2\pi\int_0^\infty\varphi n_t dr, \tag{A10}$$

where

$$\varphi\equiv-r+\frac{3}{4}\sigma_{eff}(A_p)r^2-\varepsilon\ln(n). \tag{A11}$$

From the mean field equation (26), n_t can be expressed in terms of flux,

$$n_t=-f_r, \tag{A12}$$

where

$$f=-\left(1-\frac{3}{2}\sigma_{eff}(A_p)r\right)n-\varepsilon n_r \quad \text{in} \quad r\geqslant 0 \tag{A13}$$

is the dimensionless version of flux (15). Substituting Eq. (A12) into Eq. (A10) and performing integration by parts

$$\dot{F}=2\pi\int_0^\infty\varphi f_r dr=2\pi[\varphi f]_0^\infty-2\pi\int_0^\infty\varphi_r f dr. \tag{A14}$$

Using no-flux boundary condition (16) and assuming that $f\to 0$ as $r\to\infty$, the boundary terms in Eq. (A14) disappear. In the integral,

$$\varphi_r=-1+\frac{3}{2}\sigma_{eff}(A_p)r-\varepsilon\frac{n_r}{n}=\frac{f}{n}, \tag{A15}$$

as follows from Eq. (A11). Consequently, Eq. (A14) becomes

$$\dot{F}=-2\pi\int_0^\infty\frac{f^2}{n}dr. \tag{A16}$$

The right-hand side of Eq. (A16) is less than or equal to zero, with equality only when the flux $f\equiv 0$ in $r>0$, which demonstrates that free energy F is indeed nonincreasing in time.

[1] V.F. Pastushenko, Y.A. Chizmadzhev, and V.B. Arakelyan, Bioelectrochem. Bioenerg. **6**, 53 (1979).
[2] A. Barnett and J.C. Weaver, Bioelectrochem. Bioenerg. **25**, 163 (1991).
[3] J.C. Weaver and Y.A. Chizmadzhev, Bioelectrochem. Bioenerg. **41**, 135 (1996).
[4] S.A. Freeman, M.A. Wang, and J.C. Weaver, Biophys. J. **67**, 42 (1994).
[5] J.C. Weaver and R.A. Mintzer, Phys. Lett. **86A**, 57 (1981).
[6] R.W. Glaser, S.L. Leikin, L.V. Chernomordik, V.F. Pastushenko, and A.I. Sokirko, Biochim. Biophys. Acta **940**, 275 (1988).
[7] J.C. Neu and W. Krassowska, Phys. Rev. E **59**, 3471 (1999).
[8] I.G. Abidor, V.B. Arakelyan, L.V. Chernomordik, Y.A. Chizmadzhev, V.F. Pastushenko, and M.R. Tarasevich, Bioelectrochem. Bioenerg. **6**, 37 (1979).
[9] R.P. Joshi and K.H. Schoenbach, Phys. Rev. E **62**, 1025 (2000).
[10] D.V. Zhelev and D. Needham, Biochim. Biophys. Acta **1147**, 89 (1993).
[11] O. Sandre, L. Moreaux, and F. Brochard-Wyart, Proc. Natl. Acad. Sci. U.S.A. **96**, 10591 (1999).
[12] D.C. Chang and T.S. Reese, Biophys. J. **58**, 1 (1990).
[13] H. Isambert, Phys. Rev. Lett. **80**, 3404 (1998).
[14] P. Sens and S.A. Safran, Europhys. Lett. **43**, 95 (1998).
[15] F. Brochard-Wyart, P.G. de Gennes, and O. Sandre, Physica A **278**, 32 (2000).
[16] J. Israelachvili, *Intermolecular and Surface Forces*, 2nd ed. (Academic Press, London, 1992).
[17] M. Toda, R. Kubo, and N. Saito, *Statistical Physics I* (Springer-Verlag, Tokyo, 1983).
[18] E. Zauderer *Partial Differential Equations of Applied Mathematics* (Wiley, New York, 1983).
[19] G. Dahlquist and A. Björck, *Numerical Methods* (Prentice-Hall, Englewood Cliffs, NJ, 1974).
[20] E. M. Lifshitz and L. P. Pitaevskii, *Physical Kinetics* (Perga-

mon Press, Oxford, 1981).
[21] J. D. Logan, *Applied Mathematics. A Contemporary Approach* (Wiley New York, 1987).
[22] I.P. Sugar, W. Forster, and E. Neumann, Biophys. Chem. **26**, 321 (1987).
[23] M. Hibino, M. Shigemori, H. Itoh, K. Nagayama, and K. Kinosita, Jr., Biophys. J. **59**, 209 (1991).
[24] L.L. Bonilla, J.A. Carillo, and J. Soler, Phys. Lett. A **212**, 55 (1996).
[25] C. Kittel, *Elementary Statistical Physics* (Wiley, New York, 1961).